NUMERICAL INVESTIGATION ON THE INFLUENCE OF BLADE ROOTS (STUBS) ON HOVERING ROTORS

P. Beaumier, J. Brezillon•

Applied Aerodynamics Department, ONERA, Châtillon, France

ABSTRACT

In rotary-wing problems, the numerical simulation of isolated rotors is generally concentrated on the "aerodynamic" part of the blades without taking into account the blade roots (called stubs in this paper). As a consequence, the comparison with experimental results is not straightforward since the influence of the blade roots has to be removed from the wind-tunnel measurements. In general, the experimental results are corrected by assuming that the performance of the isolated blade is equivalent to the performance of the complete rotor minus the contribution measured on the isolated stub. This hypothesis cannot be verified by using an experimental approach. The purpose of the paper is to present an original numerical study of the stub influence on rotor aerodynamic performance, by using 3D Navier-Stokes computations. This analysis gives a new insight on the validity of the correction procedures used in test for hover conditions.

NOTATION

a_∞	speed of sound at infinity
b	number of blades
Cd	2D sectional drag coefficient
CdM^3c/R	2D sectional power coefficient
Cl, ClM^2, ClM^2c/R	2D sectional lift coefficients
c_{ref}	reference chord length
$Cb=\frac{200.P}{\rho_\infty S\sigma(R\Omega)^3}$	power (or torque) coefficient
$Zb=\frac{200.T}{\rho_\infty S\sigma(R\Omega)^2}$	thrust coefficient
$Kp=\frac{p-p_\infty}{0.5\rho_\infty(r\Omega)^2}$	pressure coefficient
$M=\frac{r\Omega}{a_\infty}$	sectional Mach number
$M_{\Omega R}=\frac{R\Omega}{a_\infty}$	tip rotation Mach number
p	local pressure
p_∞	pressure at infinity
P	power consumed by the rotor
r	spanwise location
R	rotor radius
$S=\pi R^2$	rotor disk surface
T	rotor thrust
T_∞	temperature at infinity
x/c	chordwise location
μ	fluid viscosity
μ_t	turbulent viscosity
Ω	rotational angular velocity
θ_c	blade collective pitch
ρ, ρ_∞	density, density at infinity
$\sigma=\frac{bc_{ref}}{\pi R}$	rotor solidity
$\Re_{TIP}$	Reynolds number (based on tip velocity and c_{ref})

INTRODUCTION

On helicopters, the main rotor performance is essential since the blades have to provide both the lift and the propulsive forces necessary to the aircraft. Therefore, a complete understanding of the complex aerodynamic flowfield occurring around the main rotor may improve the global performance of the aircraft.

In the past, both experimental and numerical rotor studies have concerned the aerodynamic part of

• presently at the DLR Braunschweig

the blades equipped with optimized airfoils (Figure 1); the influence of the blade roots (called stubs in this paper) was always considered as a part of the fuselage drag. It is known that the hub and stubs contribution to the overall fuselage drag is important, as seen for example in the recent experimental study performed in the ONERA F1 wind-tunnel [1]. Moreover, it is known that blade roots corrections are important in rotor testing for accurate performance measurement and to correctly trim the rotor. In general, the experimental results are corrected by assuming that the performance of the isolated blade is equivalent to the performance of the complete rotor minus the contribution measured on the isolated stub. Of course, this rather simple procedure neglects the interactional effects.

The purpose of the paper is to present an original numerical study on the complete blade including the influence of the stub. The results are used to assess the validity of the experimental hub correction procedure. The study is performed in hover mode, as a first step before studying a rotor in forward flight.

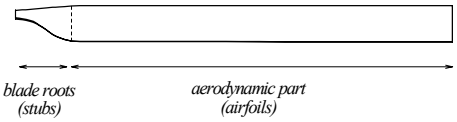

Figure 1: distinction between blade aerodynamic part and blade root

METHODOLOGY

Configurations

The configurations presented in this paper are based on the geometry of the 7A rotor. This rotor is equipped with four rectangular blades and has an aspect ratio equal to 15 with a linear twist equal to –8.3°/R. The different calculations presented here are carried out for the following conditions: $M_{\Omega R}$=0.617, $\Re_{TIP}$=1.93x10^6 and T_∞=298K.

In order to analyze the influence of the stubs, three configurations -i.e. geometries- have been investigated during this study: the isolated blade, the isolated stub and the blade with the stub respectively called C1, C2 and C3 configurations (Figure 2).

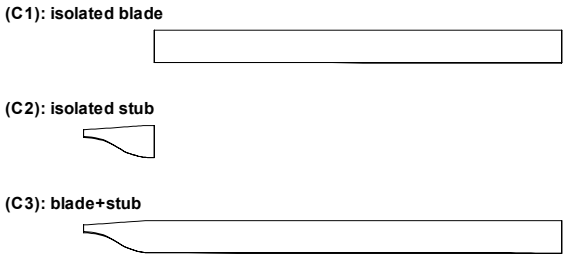

Figure 2: studied geometries

Numerical method

The *elsA* software [2] solves the Reynolds Averaged Navier-Stokes equations, written in a rotating Cartesian coordinate system. These equations are discretized in space and time following a Jameson scheme [4]. For the spatial discretization, a cell-centered volume formulation is used, which is of 2nd order accuracy on smooth grids. For the integration in time, an explicit 4th order Runge-Kutta scheme is applied. For steady applications a local time step is used and an implicit residual smoothing technique combined with a multigrid method accelerate the convergence to steady state.

For the present study, most of the calculations use the algebraic turbulence model of Michel; in the last part of this paper, calculations are carried out with the k-ω turbulence model in order to check the conclusions obtained with the Michel model. For all the computations presented here, the following standard numerical parameters have been chosen: ki2=0.5 (2nd order dissipation coefficient), ki4=0.016 (4th order dissipation coefficient), CFL=4.

For an isolated hovering multi-bladed rotor, the periodicity of the problem is used to reduce the size of the computational domain. The angle of periodicity is 2π/b, where b is the number of blades. Using this technique, special boundary conditions are applied at the periodic grid surfaces on which the flow information are transferred from the rear to the front grid boundaries and vice-versa. The boundary condition at the blade surface is the no-slip condition with adiabatic wall. This boundary condition zeroes all the components of the velocity vector at the body surface. Inboard, near the axis of rotation (hub surface), the boundary condition is a free stream condition. For this boundary, the flow variables are treated following the concept of characteristic variables for non reflecting boundary conditions. Finally, for the inflow-outflow far-field boundaries, the boundary conditions are based on the 1D momentum theory (or Froude theory [6]), already developed and used in [3].

Grid generation

Up to now, the grids used at ONERA to compute an isolated rotor in hover were analytically generated for isolated blade without stub: these grids had a C-H monoblock topology. In the present study, such a strategy cannot be used due to the almost rectangular cross section of the stub. Consequently, the ICEM-CFD software was used due to its ability to generate complex meshes around different kinds of bodies.

The grids are generated according to the CAD definition of the 7A rotor with simplified -but realistic- blade roots. The grid extension in spanwise and vertical directions was chosen in agreement with the state of the art of previous computation achieved on isolated rotor in hover: ±2R in the vertical direction and 3R in the spanwise direction. However, contrary to previous studies, the blade is not modified at the trailing edge which remains thick and the blade tip is not truncated.

The grid topology is constructed for Navier-Stokes computations and remains the same for the three configurations C1, C2 and C3. An O-O type mesh surrounds the blade with grid points clustering near the blade surface to allow an accurate discretisation of the boundary layer. Further from the blade, the domain is gridded with a concatenation of H type blocks up to the outer boundaries. The O grid has 41 points in the direction orthogonal to the blade surface; each section of the rotor has 113 grid points in the chordwise direction and 33 grid points at the trailing edge. In total, the mesh is split into 7 blocks which cover an azimuthal sector of 90°. The mesh size depends on the geometry and varies between approximately 775.000 points for the isolated stub (C2) to 1.110.000 points for the complete blade (C3).

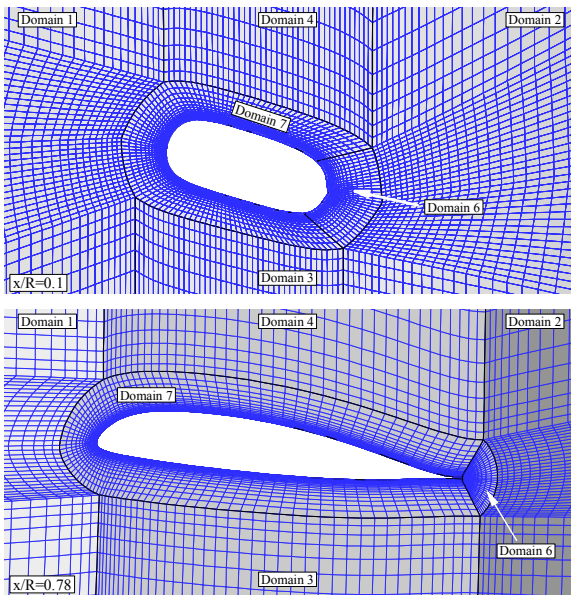

Figure 3: Grid topology around sections of the stub (top) and of the blade (bottom)

For each configuration, grids have been generated for three collective pitch angles:

- θ_c=5.97°: low thrust,
- θ_c=8.94°: medium thrust,
- θ_c=10.5°: high thrust.

ANALYSIS OF COMPUTATIONAL RESULTS

Isolated blade: influence of grid topology

In a first part, the numerical flow solution obtained on the new multiblock topology is compared with standard solutions obtained previously on a conventional monoblock grid, in order to check that the main features of hovering rotors are well captured by the new gridding technique. This comparison is done for the low thrust case defined by θ_c=5.97°. The convergence of total thrust and torque coefficients plotted in Figure 4 show that both solutions are well converged after no more than 1000 multigrid cycles. The converged value of rotor thrust is slightly higher (ΔZb=0.3) with the new multiblock grid compared to the monoblock grid. This is checked in Figure 5 where the spanwise evolution of sectional loads and power coefficients are represented: despite a very similar spanwise evolution (which is remarkable), it can be seen that the sectional lift coefficients (ClM^2c/R) in the new grid are slightly higher than in the standard grid; this is also true for the sectional power coefficients CdM^3c/R, especially between r/R=0.9 and r/R=1. One part of the differences observed near the tip is a consequence of the blade tip geometry, which is better represented by the new grid than by the standard one. The other differences observed all along the span are a consequence of the trailing-edge representation: indeed, some very small vortices (Figure 6) are captured behind the trailing-edge of the new grid because of the representation of the trailing-edge thickness, which was assumed to be zero in the standard monoblock mesh.

The differences mentioned above are observed for all the pitch angles studied in this paper. It can be concluded that some expected differences have been found between the monoblock and multiblock topologies. However, these differences appear to be small (ΔZb=0.3, whatever the pitch angle is) so that the solution on the new multiblock grid can be considered as validated.

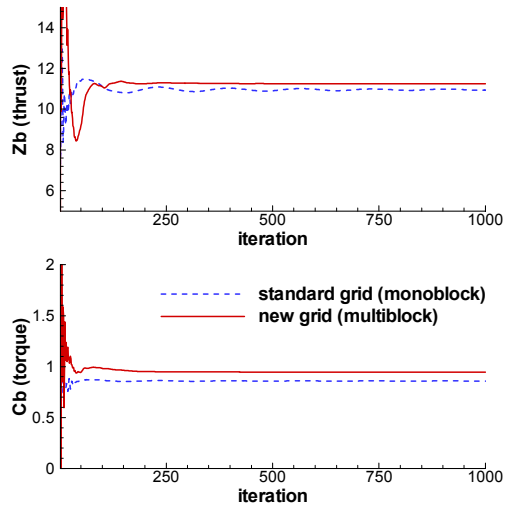

Figure 4: Convergence of total thrust (top) and torque (bottom) coefficients

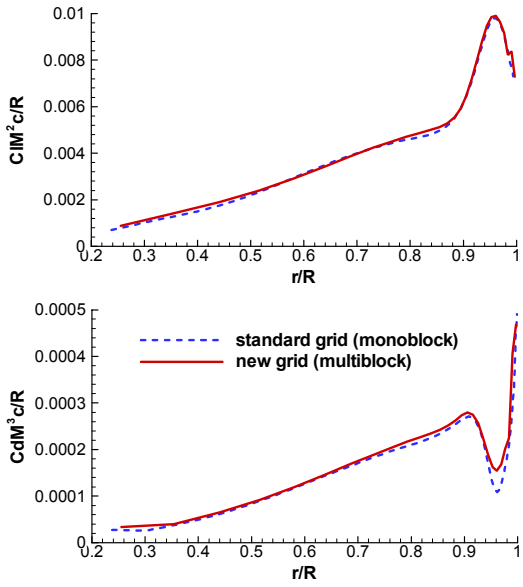

Figure 5: Influence of grid topology on 2D sectional lift (top) and power (bottom) distribution

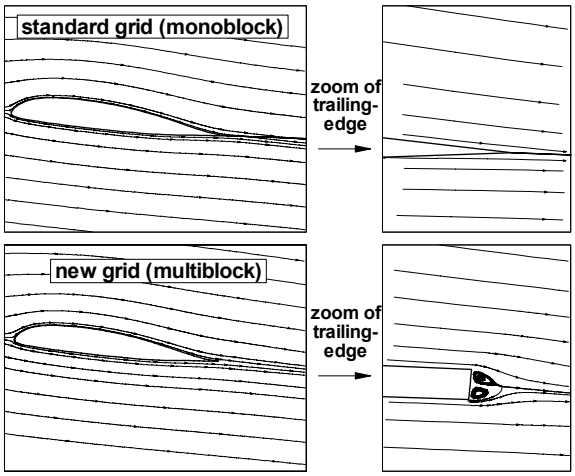

Figure 6: Streamlines near trailing-edge

Solution on the blade (with and without stub)

In this paragraph, one compares the numerical solutions on the blade without and with the presence of the stub. The solution without the stub is obtained by an "isolated blade" calculation (configuration C1) and the solution with the stub is obtained by a calculation on configuration C3. A detailed comparison of the two solutions is done for the low thrust case (θ_c=5.97°) and additional comments are then done for the other test cases.

The first result is that the total thrust in the "blade+stub" configuration is slightly lower than in the isolated blade configuration (Figure 7, top), which is somewhat unexpected since the presence of the stub should generate some additional lift. Similarly, Figure 7 shows that the power consumed by the "blade+stub" is slightly lower than in the isolated blade case, which is consistent with the lower value of the total thrust. A first explanation of this result is provided by Figure 8, representing the 2D sectional lift distributions in terms of C_l (top) and C_lM^2 (bottom) coefficients. The corresponding pressure distributions are plotted in Figure 9. The lift distributions of the two configurations are identical from r/R=0.5 up to r/R=1, and differ only in the inner part of the blade: from r/R=0.22 to 0.5, the C_l coefficients are higher on the isolated blade compared to the "blade+stub" configuration. Of course, the stub generates some additional thrust but not enough to compensate for the loss of thrust around r/R=0.3, so that there is less total thrust on the "blade+stub" configuration than on the isolated blade. Note that the high values of C_l coefficients on the stub (up to C_l=1.6) do not contribute significantly to the total rotor thrust because of the low rotational velocities of the sections located near the axis of rotation compared to the outboard sections.

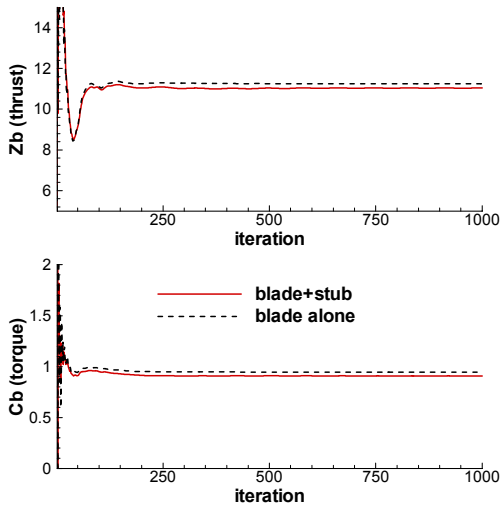

Figure 7: Influence of stub on total thrust and torque coeffficients (θ_c=5.97°)

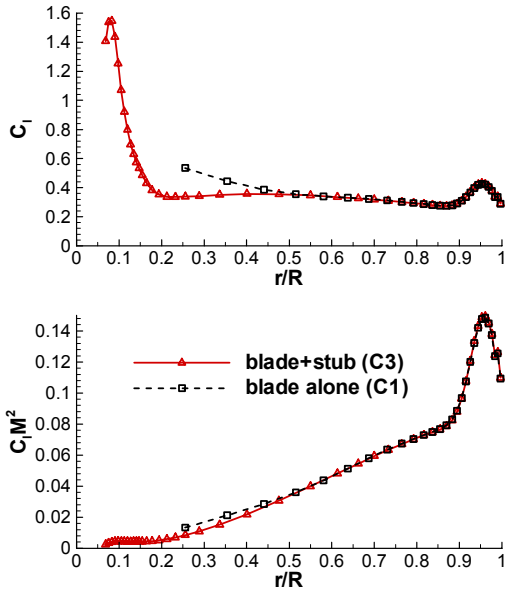

Figure 8 : Influence of stub on 2D sectional lift coefficients (θ_c=5.97°)

A good understanding of the different physical phenomena occuring on the two configurations C1 and C3 is provided by Figure 10, representing contour levels of vorticity in a vertical plane located 10° behind the blade. In both configurations, the tip vortex, the vortex of the preceding blade and the wake sheet can be clearly seen; the development of these structures and the wake contraction are almost identical in the two cases. Some differences appear behind the stub, where an inner wake contraction is obtained in configuration C3 (blade+stub) because of the generation of an inboard vortex which has an opposite sense of rotation compared to the tip vortex. This explains the lift reduction obtained around r/R=0.3 on the "blade+stub" configuration.

The differences between configurations C1 and C3 in terms of total thrust or torque have been found almost insensitive to collective pitch angles. They can be quantified by the following numbers: ΔZb=0.2, ΔCb=0.04. This represents a relative difference of 1 to 2% in terms of thrust and between 2 to 3.5% in terms of power (the highest percentage obtained for the lowest pitch angle). This shows that an "isolated blade" calculation is in fact very close to a "blade+stub" calculation in terms of total thrust or power.

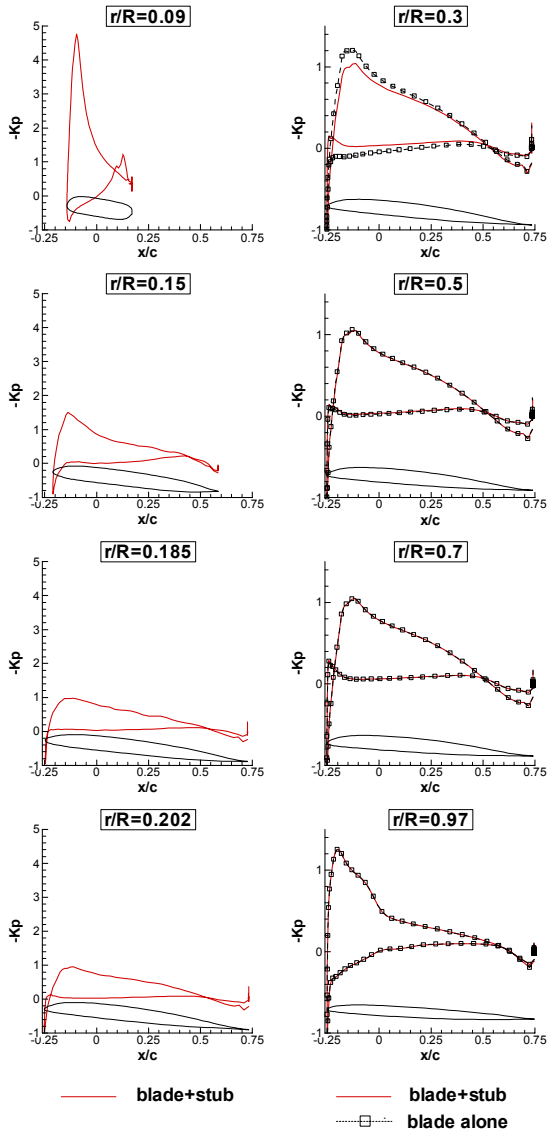

Figure 9: Influence of stub on pressure distributions (θ_c=5.97°)

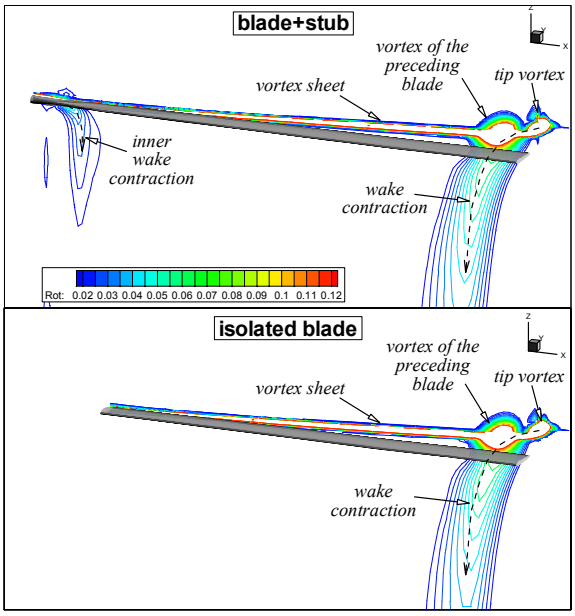

Figure 10: Vorticity field with and without stub (θ_c=5.97°)

Solution on the stub (with and without blade)

In this part, one compares the numerical flow solution around the isolated stub (C2 configuration) and around the complete blade (C3 configuration). This comparison gives some indication on the validity of the experimental approach to deduce the rotor performance. The conclusion, drawn for the lowest thrust case, remains unchanged for the other cases.

For the C2 and C3 configurations, the main aerodynamic differences are analysed by comparing the pressure distributions at 4 sections located on the stub (Figure 11). It can be noticed that the pressure on the upper side of the "blade+stub" configuration is always the lowest, except at the tip of the isolated stub (r/R=0.202). Similarly, on the lower side of the C3 configuration, the pressure level is significantly larger than on the C2 configuration, for r/R<0.202. The corresponding sectional lift coefficient Cl is thus higher for the C3 configuration than for C2, except on the stub tip for r/R>0.2 where an important increased lift occurs due to 3D effects (Figure 12).

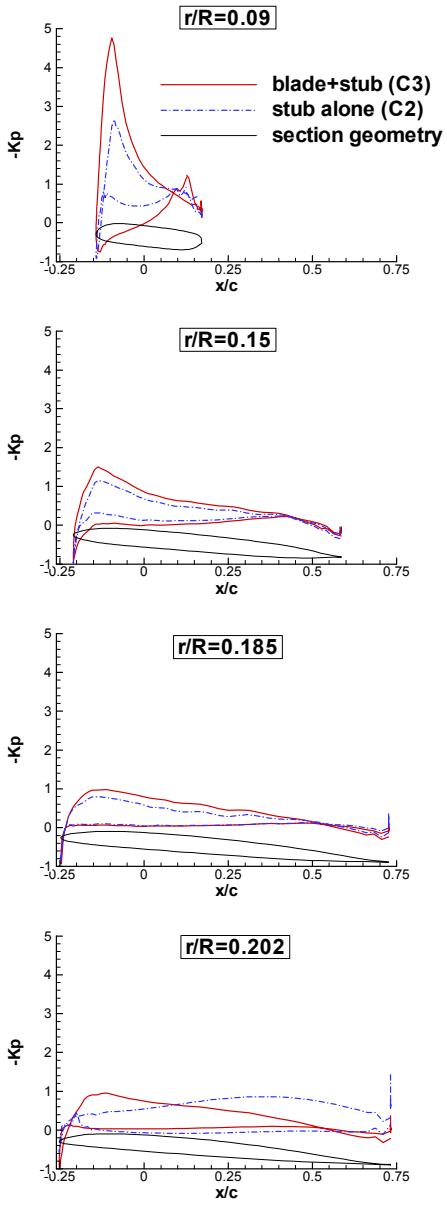

Figure 11: Pressure distribution on the stub

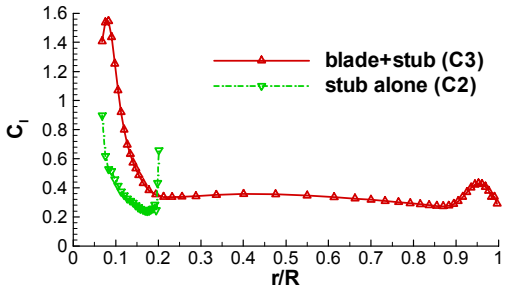

Figure 12: Lift distribution on the stub without (C2) and with (C3) blade

In fact, the 3D effects which occur on the isolated stub are of the same nature as the effects observed on the blade tip. Figure 13 shows the vorticity field in a vertical plane located 10° behind the stub: the tip vortex, the vortex of the preceding blade and the wake contraction can be clearly seen, which are of the same type as on the blade tip (Figure 10). On the contrary, it was shown in the previous part that an inboard vortex is observed on the C3 configuration (blade+stub) which produces an inner wake contraction: it can be concluded that the main aerodynamic difference between the isolated stub (C2) and the complete blade (C3) is the sense of rotation of the vortex which occurs behind the stub part.

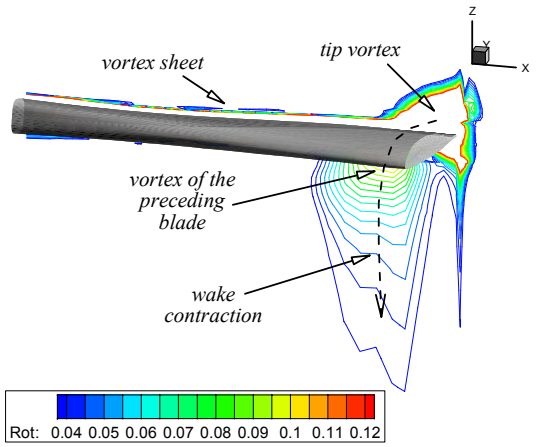

Figure 13: Vorticity field in a vertical plane located 10° behind the isolated stub

One can assume that the vortex sense of rotation should play an important role on the flowfield around the stub. This is shown on Figure 14 with the streamlines around the stub section located at r/R=0.09 for the C2 and C3 configurations. The inner vortex, generated behind the "blade+stub" configuration, induces a slight upwash, illustrated by the streamlines orientation from bottom to top (Figure 14, top): this results in a higher local incidence compared to the local incidence induced by the outer vortex of the stub alone. On the contrary, in configuration C2 (Figure 14, bottom), the stub tip vortex creates a downwash illustrated by the streamlines orientation from top to bottom. The higher local incidence in configuration C3 induces a higher local lift, which is in agreement with previous remarks (Figure 12). Another consequence of a higher angle of incidence concerns the flow separation which can occur on such a geometry. This feature is illustrated by Figure 15 which compares the skin friction lines on the C2 and C3 configurations. In configuration C3, a separation occurs on the upper surface of the stub while it is not the case in configuration C2.

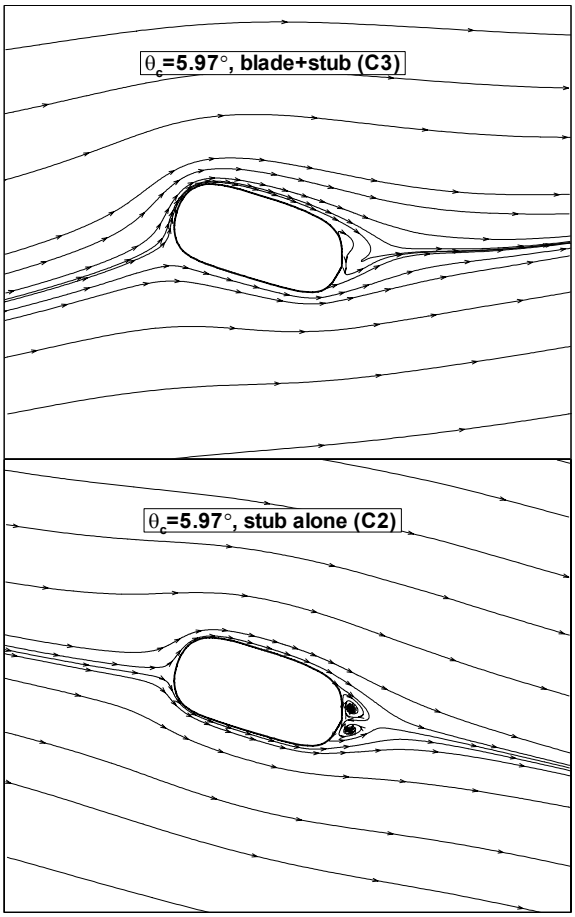

Figure 14: Streamlines around one of the stub section (r/R=0.9) in configurations C3 and C1

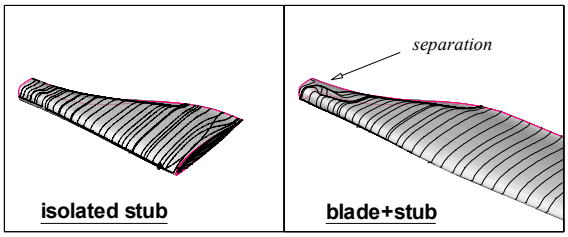

Figure 15: Skin friction lines on the "blade+stub" (C3) and on the isolated stub (C2) configurations (θ_c=5.97)

In the calculations performed for higher collective pitch angles, the features described previously are amplified: on the isolated stub configuration, the sectional lift coefficients increase and larger separation occurs on the stub part of the C3 configuration.

Influence of turbulence model

All the calculations presented so far have been carried out using an algebraic turbulence model (Michel), the validity of which may be questionable, especially when unattached flows are computed. In this part, computations for the medium thrust case (θ_c=8.94°) are repeated with the 2-equation k-ω turbulence model available in the *elsA* code. Previous studies already validated the use of this model for isolated rotors in hover by comparison with the solutions obtained with the Michel algebraic model and also with experiment, for a wide range of thrust levels. The purpose of this part is to check that the conclusions drawn in the preceding paragraphs are still valid with the k-ω model.

A first analysis of the flow solution (Figure 16) shows that the turbulent contour levels (μ_t/μ) obtained with the k-ω turbulence model is more physical than the one obtained with the algebraic model. In fact, the multiblock topology does not allow to apply the Michel model in the blocks not attached to the blade surface: the turbulent viscosity is then assumed to be equal to 0, which is of course erroneous. On the contrary, the computation with the k-ω model shows a continuous field of turbulent viscosity, both around a section of the stub (left part of Figure 16) and around a section of the blade (right part of Figure 16). It can be noticed that the turbulence generated by the preceding blade is visible in the k-ω solution, for the blade section represented in Figure 16 (bottom, right).

It can also be checked that a large area of unattached flow is found on the stub in configuration C3, which is not the case in configuration C1 (Figure 17). This confirms the qualitative results obtained with the Michel model, even if the area of reversal flow is more pronounced in the k-ω calculation than in the Michel calculation.

From a quantitative point of view, the results obtained with the k-ω turbulence model in terms of total thrust and power coefficients are similar (although not absolutely identical) to the results obtained with the Michel model. More precisely, the "blade+stub" configuration shows a thrust reduction ΔZb/Zb=1.8% (instead of ΔZb/Zb=1.1% with the Michel model) and a power reduction ΔCb/Cb=1.6% (instead of ΔCb/Cb=2.7% with the Michel model).

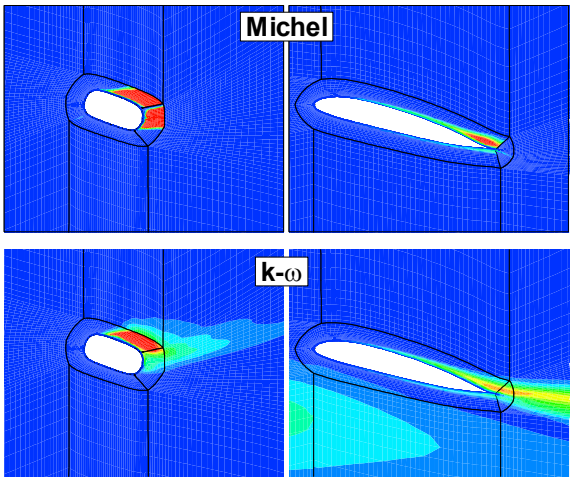

Figure 16: Contour levels of turbulence (μ_t/μ) with algebraic (top) and k-ω (bottom) turbulence models (θ_c=8.94°)

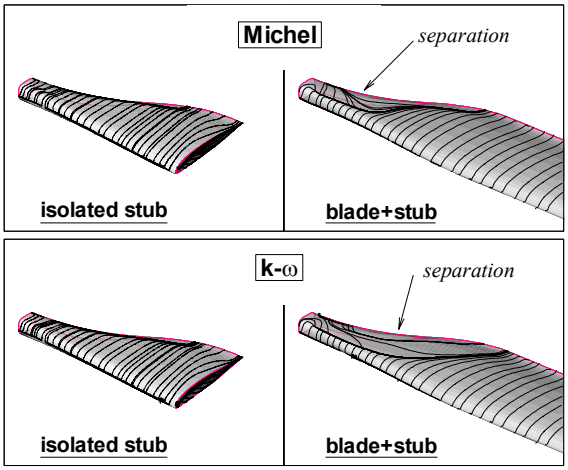

Figure 17: Skin friction lines on the "blade+stub" (C3) and on the isolated stub (C1) configurations (θ_c=8.94°)

Synthesis

Thanks to the calculations performed in this study, it is possible to address the problem mentioned at the beginning of this paper concerning the "hub correction procedure". In experiment, it is assumed that the performance of the aerodynamic part of the blade is equal to the performance of the complete rotor minus the contribution measured on the isolated stub. The same kind of procedure is applied in the present calculations in order to estimate whether the symbolic equation: (blade)=(rotor)-(stub) is valid or not.

Figure 18 compares the thrust and power coefficients of the aerodynamic part of the blade in the "blade+stub" configuration with the difference between what is computed in the "blade+stub" configuration (C3) and in the "isolated stub" configuration (C2). Concerning the thrust coefficient, there is almost no difference between the

two methods for extracting the thrust contribution of the aerodynamic part of the blade. This means that the hub correction procedure is valid with an accuracy which is better than 0.5%. As far as the power is concerned, the error ranges between 1 and 2% depending on the collective pitch. This difference is small but not negligible.

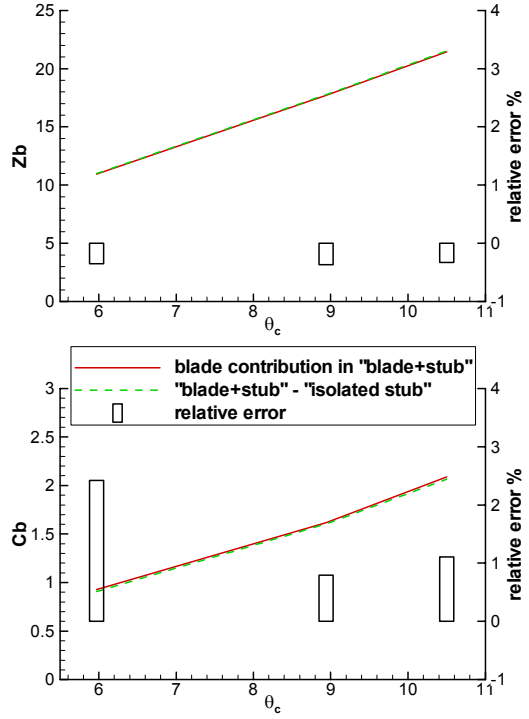

Figure 18: Evaluation of "hub correction procedure"

CONCLUDING REMARKS

The influence of the blade roots (stubs) on the performance of a helicopter rotor in hover has been studied by running Navier-Stokes computations on three different configurations: isolated blade (C1), isolated stub (C2) and blade+stub (C3). The calculations carried out with the *elsA* software using either an algebraic turbulence model (Michel) or a 2-equation turbulence model (k-ω) give a better understanding of the influence of the stub. From the computed solutions at different blade collective pitch angles in hover, the following main conclusions can be drawn:

- the total thrust computed on a "blade+stub" configuration is between 1% and 2% lower than on an isolated blade; this is a consequence of a vortex of small intensity generated by the stub, with an opposite sense of rotation compared to conventional tip vortices;

- as far as forces are concerned, it is reasonable to assume that the contribution of the aerodynamic sections of the "blade+stub" configuration can be estimated by subtracting the forces on the isolated stub from the total forces on the "blade+stub" configuration; this validates the "hub correction procedure" used in experiments for hover configurations;

- the flowfield around an isolated stub has been found fundamentally different from that observed on a complete "blade+stub" configuration; in the later case, large area of reversal flows have been predicted, which is not the case on an isolated stub because of the generation of a stub tip vortex.

Continuation of this work will mainly concern forward flight applications for which the standard experimental "hub correction procedure" should be checked in detail, especially as far as the total rotor drag force is concerned.

ACKNOWLEGDEMENT

The authors would like to acknowledge the French Agency for Civil Aviation DGAC for their financial support and A. Faubert for performing the k-ω computations.

REFERENCES

[1] Helicopter Fuselage Drag, HELIFUSE SYNTHESIS REPORT, July 1999

[2] Boniface, J.C., Cantaloube, B., Jollès, A., "Rotorcraft simulations using an Object Oriented approach.", 26th European Rotorcraft Forum, The Hague (The Netherlands), September 2000

[3] Beaumier, P., Chelli, E., Pahlke, K., "Navier-Stokes prediction of helicopter rotor performances in hover including aero-elastic effects". 56th AHS Forum, Virginia Beach (USA), May 2000

[4] Jameson, A., Schmidt, W., Turkel, E., "Numerical Solution of the Euler Equations by Finite Volume Methods using Runge-Kutta Time Stepping Schemes", AIAA Paper 81-1259, 1981

[5] Michel, R., Quémard, C., Durant, R., "Application d'un schéma de longueur de mélange à l'étude des couche limites turbulentes d'équilibre", ONERA NT 154, 1969

[6] Horlock, J.H., "Actuator Disk Theory", Mac Graw-Hill, 1978